HHS Public Access

Author manuscript

J Am Soc Mass Spectrom. Author manuscript; available in PMC 2024 June 08.

Published in final edited form as:

J Am Soc Mass Spectrom. 2023 October 04; 34(10): 2232–2246. doi:10.1021/jasms.3c00187.

Top-down protein analysis by tandem-trapped ion mobility spectrometry / mass spectrometry (tandem-TIMS/MS) coupled with ultraviolet photodissociation (UVPD) and parallel accumulation/serial fragmentation (PASEF) MS/MS analysis

Fanny C. Liu[1], **Mark E. Ridgeway**[2], **Christopher A. Wootton**[3], **Alina Theisen**[3], **Erin M. Panczyk**[2], **Florian Meier**[4], **Melvin A. Park**[2], **Christian Bleiholder**[*,5]

[1]Department of Chemistry and Biochemistry, Florida State University, Tallahassee, FL 32304, USA

[2]Bruker Daltonics, Billerica, MA, 01821, USA

[3]Bruker Daltonics, 28359 Bremen, Germany

[4]Functional Proteomics, Jena University Hospital, 07747 Jena, Germany

[5]Institute of Molecular Biophysics, Florida State University, Tallahassee, FL 32304, USA

Abstract

‘Top-down’ proteomics analyzes intact proteins and identifies proteoforms by their intact mass as well as the observed fragmentation pattern in tandem mass spectrometry (MS/MS) experiments. Recently, hybrid ion mobility spectrometry-mass spectrometry (IM/MS) methods have gained traction for top-down experiments, either by allowing top-down analysis of individual isomers or alternatively by improving signal/noise and dynamic range for fragment ion assignment. We recently described the construction of a tandem-trapped ion mobility spectrometer/mass spectrometer (tandem-TIMS/MS) coupled with an ultraviolet (UV) laser and demonstrated proof-of-principle for top-down analysis by UV photodissociation (UVPD) at 2–3 mbar. The present

[*]**Address reprint requests to:** cbleiholder@fsu.edu, Christian Bleiholder, Florida State University, Department of Chemistry and Biochemistry, Tallahassee, FL 32304.

1. Fanny Caroline Liu, Florida State University, Tallahassee, Florida 32304, United States
2. Mark E. Ridgeway-Bruker Daltonics, Billerica, Massachusetts 01821, United States
3. Christopher Andrew Wootton-Bruker Daltonics, 28359 Bremen, Germany
4. Alina Theisen-Bruker Daltonics, 28359 Bremen, Germany
5. Erin M. Panczyk-Bruker Daltonics, Billerica, Massachusetts 01821, Unites States
6. Florian Meier-Functional Proteomics, Jena University Hospital, 07747 Jena, Germany
7. Melvin A. Park-Bruker Daltonics, Billerica, Massachusetts, United States
8. Christian Bleiholder-Florida State University, Tallahassee, Florida 32304, United States

Author Contributions

The manuscript was written through contributions of all authors. All authors have given approval to the final version of the manuscript.

Supporting Information.

10 figures showing mass spectra and ion mobility spectra of the studied protein systems.

work builds on this with an exploration of a top-down method that couples tandem-TIMS/MS with UVPD and a parallel-accumulation serial fragmentation (PASEF) MS/MS analysis. We first survey types and structures of UVPD-specific fragment ions generated at the 2–3 mbar pressure regime of our instrument. Notably, we observe UVPD-induced fragment ions with multiple conformations that differ from those produced in the absence of UV irradiation. Subsequently, we discuss how MS/MS spectra of top-down fragment ions lend themselves ideally for probability-based scoring methods developed in the bottom-up proteomics field and how the ability to record automated PASEF-MS/MS spectra resolves ambiguities in assignment of top-down fragment ions. Finally, we describe coupling of tandem-TIMS/MS workflows with UVPD and PASEF-MS/MS analysis for native top-down protein analysis.

Graphical Abstract

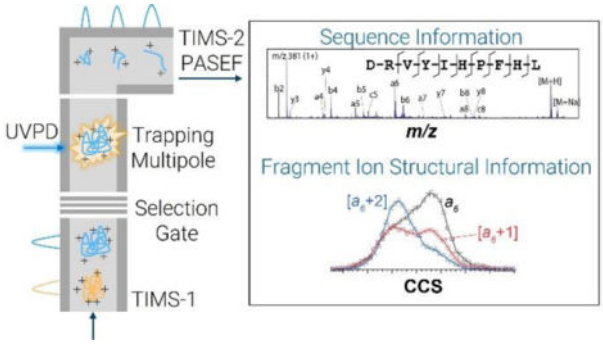

Introduction

During gene expression, mechanisms such as alternative splicing of transcripts and post-translational modification of proteins can give rise to different molecular forms of a protein (so-called proteoforms).[1,2] Proteoforms lead to remarkable structural and functional diversity of a typical mammalian cell[3,4] with current estimates of over one million proteoforms.[5,6]

Mass spectrometry (MS) has become increasingly successful in disentangling the complexity of proteomes.[7] Typically, proteins are extracted from a biological sample of interest and enzymatically digested to peptides, which are then separated *via* liquid chromatography and mass analyzed. This ‘bottom-up’ approach routinely quantifies thousands of proteins in a single experiment and scales to a large number and broad range of samples. However, an immediate consequence of this workflow is that the link of peptides originating from the same protein molecule, i.e. the proteoform information, is not conserved. By contrast, ‘top-down’ proteomics analyzes intact proteins.[8] Proteoforms are then identified by their intact mass as well as the observed fragmentation pattern in tandem mass spectrometry (MS/MS) experiments, providing insight into sequence variants as well as the localization of post-translational modifications and their co-occurrence within distinct proteoforms.[9–12]

In practice, however, the complexity of the proteome renders top-down protein analysis technologically challenging.[13] Achieving complete sequence coverage of intact proteins, a

prerequisite for localizing all potential proteoforms, demands that a single precursor protein is cleaved at hundreds of peptide bonds to produce sequence-informative fragment ions. This often results in low signal/noise ratios and overlapping isotope distributions of the fragment ions due to dilution of a finite number of precursor protein ions into different fragment ions, charge states, and isotopes.[14] These challenges are exacerbated by protein (in)solubility[15] and a very high dynamic range.[5] To resolve these challenges, most top-down experiments are carried out with Fourier transform (FT)-based instruments that achieve extremely high resolving powers and mass accuracies. Parallel improvements in separation of intact proteins prior to MS analysis,[16–18] MS sensitivity,[19] MS/MS fragmentation[20–22] of large proteins and protein complexes, and enrichment of specific protein precursor charge states[23] have greatly increased sequence coverages achieved in top-down experiments.[10]

More recently, hybrid ion mobility spectrometry-mass spectrometry (IM/MS) methods have gained traction for top-down experiments.[20,24–27] IMS separates ions according to differences in their ion mobilities, K, when the ions traverse an inert buffer gas under the influence of an applied electric field.[28,29] One application of IM/MS in conjunction with top-down experiments is to separate intact proteins prior to their MS/MS fragmentation.[27] This strategy enables top-down analysis of mobility-selected conformations and/or proteoforms, as recently described by Bethias *et al.* for mobility-separated, permuted histone tails.[30] Another application of IM/MS is to separate the top-down fragment ions produced by MS/MS fragmentation,[20,24–27,31,31–37] thereby improving signal/noise and dynamic range for assignment of the fragment ions. Furthermore, knowledge of cross sections of top-down fragment ions may be useful for their assignments[37] in line with strategies developed for bottom-up proteomics.[38,39] Nevertheless, the time-scale of IMS (<200 ms) makes it ideally suited for coupling to time-of-flight (TOF) mass analyzers rather than FT-MS. Consequently, fidelity of fragment ion assignment in top-down protein experiments by such IMS/TOF instruments is limited by the mass resolution and accuracy achievable by the TOF analyzer.

Tandem-IM/MS methods couple multiple ion mobility separations with ion dissociation in a single instrumental setup.[40–49] Hence, such an approach has the potential of coupling top-down analysis of mobility-selected proteoforms with the benefits of mobility-separating fragment ions for their assignments, such as improved signal/noise and dynamic range. Such measurements can also be carried out from native solution conditions,[31,37,40,45,50] thereby raising the possibility of correlating the presence of proteoforms with differences in protein structure and, thus, function.

Our own laboratories previously reported on the development of tandem-trapped ion mobility spectrometry/mass spectrometry (tandem-TIMS/MS)[40,51,52] and discussed application of the method to study peptide oligomers,[53] native-like structures of proteins and their complexes,[31,35,50,54] sequence analysis of carbohydrates,[55] and top-down analysis of proteins and protein complexes.[31,36,37,40] At first constructed from co-axially coupling two prototype TIMS devices enabling only CID for precursor ion dissociation,[40] we subsequently developed an orthogonal tandem-TIMS/MS configuration that we coupled with a 213 nm UV laser for UV photodissociation (UVPD).[36] We demonstrated proof-of-principle for UVPD of intact proteins at the 2–3 mbar pressure regime compatible with

TIMS and to mobility-separate the top-down fragment ions generated by CID and/or UVPD.[36] These abilities were subsequently confirmed by Dit Fouque *et al.* and applied to sequence analysis of histone samples.[56] The specific tTIMS/MS-UVPD instrument[36] reported by us was constructed from a commercial timsTOFPro instrument and therefore enables parallel accumulation/serial fragmentation (PASEF) workflows[57] for the fragment ions generated from UVPD.

In the present paper, we explore the potential of tandem-TIMS/TOF-CID/UVPD-PASEF experiments for top-down analysis of proteins as illustrated in Scheme 1. First, we characterize background signal produced by UV irradiation of the instrument components and discuss types and structures of UVPD-specific fragment ions generated at the 2–3 mbar pressure regime of our instrument. Second, we survey the challenges associated with reliably assigning fragment ions produced from coupling UVPD and CID in effective MS^3 experiments at the 5 – 20 ppm mass accuracy achieved by current TOF mass analyzers. Third, we discuss our strategy to overcome these limitations by taking advantage of three properties of our tandem-TIMS/MS setup: (1) the ability to record MS/MS spectra resolves ambiguities in ion assignment; (2) the knowledge of the precursor ion mobility and m/z ratio limits the possible number of precursor ions for spectral matches; and (3) MS/MS spectra of top-down fragment ions lend themselves ideally for probability-based scoring methods developed in the bottom-up proteomics field. Finally, we present proof-of-principle of coupling tandem-TIMS/MS workflows with UVPD and PASEF-MS/MS analysis for native top-down analysis of proteins.

Methods

Materials and sample preparations.

Ammonium acetate, bovine ubiquitin, and bovine carbonic anhydrase II were obtained from Sigma-Aldrich (St. Louis, MO) and ESI tuning mix from Agilent (Santa Clara, CA). Native protein samples were prepared in 100 mM ammonium acetate solution at a concentration of 5 μM. Non-native protein samples were prepared in 50:50 methanol:water at a concentration of 5 μM with 1% acetic acid. ESI tuning mix was used as obtained for mass and ion mobility calibration.

Tandem-TIMS/MS (tTIMS/MS) instrumentation.

Experiments were performed on an orthogonal tandem-TIMS/MS instrument coupled with a UV laser described in detail earlier (see Figure S1, Supporting Information).[36] Briefly, this orthogonal tandem-TIMS/MS was constructed from modifying a commercially available timsTOF Pro instrument (Bruker Daltonics, Billerica, MA) by (1) incorporating an additional TIMS device between the electrospray capillary and the one already present in the timsTOF Pro; (2) inserting a linear ion trap operating at 2–3 mbar in-between the two TIMS devices; and (3) incorporating a 213 nm laser beam produced from the 5^{th} harmonic of a Nd:YAG laser. For analysis, ions are first separated by mobility in TIMS1 (Scheme 1). As the ions elute from TIMS1, in accordance with their mobilities, they may be selected and collisionally activated as described previously,[31,36,37,40] i.e. by timing the electric potentials on electrodes L1 and L2 for ion selection and by placing a voltage difference of 180 V

between apertures L2 and L3 for collisional activation of the selected ions. More technical details can be found in the original reports on TIMS[58–63] and tandem-TIMS.[36,40,51] Samples were infused into the electrospray ionization (ESI) source in positive mode through a gastight syringe. Ion mobilities and cross sections were calibrated as described for nitrogen gas.[63–66]

Parallel-accumulation / serial fragmentation tandem mass spectrometry (PASEF-MS/MS) analysis of top-down fragment ions.

We used the parallel-accumulation / serial fragmentation tandem mass spectrometry (PASEF-MS/MS) method[57,67] to perform MS/MS analysis of top-down fragment ions eluting from TIMS-2. To this end, suitable top-down fragment ions eluting from TIMS-2 were selected as precursor ions for PASEF-MS/MS in real time from TIMS-MS survey scans by a PASEF scheduling algorithm described in detail elsewhere.[57] Note that the signal intensity of top-down fragment ions is generally lower than the signal intensity of tryptic peptides or intact proteins. Hence, to enable top-down protein analysis using effective MS^3 workflows, we increased the number of TIMS-MS survey scans to 250 and the number of MS/MS repetitions to 500 per PASEF cycle, respectively. We further reduced the minimum threshold intensity for scheduling to 50 arbitrary units (a.u.) and increased the scheduling target intensity to 200,000 a.u. Additionally, we set PASEF to ignore the charge state when scheduling ions for MS/MS. These settings allowed the PASEF algorithm to (1) successfully schedule fragment ions eluting from TIMS-2 for MS/MS analysis and (2) to accumulate sufficient MS/MS spectra for the top-down fragment ions to achieve signal-to-noise ratios suitable for reliable ion assignment. CID of the scheduled ions was performed at a bias of 55 V between the quadrupole and the collision cell (no attempt was made to optimize the collision energy for different precursor charge states). The time-scale for ion mobility separation in TIMS-2 was varied from 100 ms and 300 ms while keeping the duty cycle fixed at 100%. The time-scale for ion mobility separation in TIMS-1 was set identical to that of TIMS-2. As described,[67] we used a polygon filter to restrain the m/z and ion mobility range for selection of features most likely representing top-down fragment ions rather than precursors or background ions. The m/z resolving power of the MS/MS spectra was estimated to approximately 45,000.

Data analysis.

Basic manual data analysis and visualization was carried out using Data Analysis 5.1 (Bruker Daltonics) and ProteinProspector (UCSF, San Francisco, CA) as described.[36] Top-down protein analysis of PASEF-MS/MS spectra was conducted with a home-built software algorithm described in the main text. The timsdata library provided by Bruker Daltonics was used to compile MS/MS spectra for the precursor ions by aggregating raw (profile) data MS/MS TOF scans for precursor ions within user-defined tolerances for m/z ($\delta(m/z) = 2$ Th) and ion mobility K_0 ($\delta(K_0) = 0.05$ cm^2/Vs). We used a continuous wavelet transform (CWT) for feature detection as described below, and implemented the dynamic noise level method[68] for subsequent feature reduction. MSDeconv was used for deconvolution of MS/MS spectra.[69] We implemented the open mass spectrometry scoring algorithm (OMSSA)[70] using the Apfloat library for arbitrary precision arithmetic to calculate a score

for each spectral match. The workflow was implemented in the Java programming language and is available upon reasonable request to the authors.

Results and Discussion

Collision cross sections of UVPD-specific fragment ions

We previously applied our tandem-TIMS/MS instrument to demonstrate the feasibility of performing UV photodissociation in the 2–3 mbar pressure regime compatible with TIMS and highlighted the potential of this approach for top-down protein analysis.[36] Prior to applying our UVPD / tandem-TIMS/MS setup for protein sequence analysis, however, we first characterize the ions produced under these conditions in greater detail. Our motivation here is two-fold: First, the quadrupolar ion trap and the TIMS devices here are constructed from printed circuit boards (PCBs). Irradiation of such boards with 213 nm photons at laser pulse energies on the order of ~100 μJ could potentially ionize layers of the PCBs. Such ionization events could lead to the formation of contaminant ions that would emerge as noise peaks and hence potentially degrade spectral quality and interfere with data analysis. Second, our UVPD experiments are carried out at 2–3 mbar which is much higher than the $<10^{-2}$ mbar regime for which the UV photodissociation chemistry of peptides has been rigorously discussed.[21,71–77] As described previously,[36] the elevated pressure may collisionally cool and stabilize fragment ions that may not survive to detection in other instruments that operate at lower pressures. Hence, we seek to characterize the UVPD-generated ions both in terms of the types formed and their structures.

First, we assess the abundance of contaminant ions generated by UV irradiation of the instrument components. To this end, we recorded nested ion mobility / mass spectra for angiotensin I produced by UV irradiation to the corresponding spectra that were produced with ESI and/or UVPD turned off (Figures S2 and S3, Supporting Information). Figure S2B (Supporting Information) shows that UV irradiation of the instrument (with ESI turned off) produces background ions mainly between *m/z* 100 and *m/z* 750. The intensity of the background ions increased when the laser pulse energy was increased from 4 μJ to 45 μJ. This observation supports the conclusion that these ions are generated by UV irradiation of instrument components. Nevertheless, the abundances of these background ions are roughly two to three orders of magnitude lower than the analyte-related ions observed when ESI and/or UVPD are turned on (Figures S2 and S3, Supporting Information). Figure S3 (Supporting Information) underscores that the UV-generated background ions are negligible in comparison to fragment ions produced by UV irradiation of singly- and doubly-protonated angiotensin I. We emphasize that UVPD of singly- and doubly-protonated 10-residue peptide ions is typically a low-efficiency process. Hence, our data suggest that our instrumental configuration generates UV-generated background ions of sufficiently low abundance that they generally will not interfere with analysis of fragment ions produced from analyte ions.

To characterize the UVPD dissociation chemistry in our elevated pressure regime, we assigned the fragment ions produced from UVPD of angiotensin I. Figure 1A shows the nested ion mobility / mass spectrum generated by irradiating angiotensin I by approximately 10 UV pulses at pulse energies of 45 μJ at 213 nm. The nested spectrum exhibits three

main bands of ions, of which the center band contains a sufficient number of sequence-informative fragment ions. We next identified fragment ions in the nested ion mobility/mass spectrum as described previously by first cross-correlating the nested spectrum to the isotopic pattern calculated for the fragment ions and further manually validating all fragment ion assignments.

We identified sequence-informative fragment ions both from the N-terminus (*a*, *b*, *c* - type ions) and the C-terminus (mainly *y*-type ions). As described previously, the data show abundant formation of [*a*+k] and [*y*-k] type ions with k=1, 2. We were unable to identify *z*-type ions in the spectrum and *x*-type ions appear to be of significantly lower abundances than their *y*-type congeners (see Figure 1B). The observation of *x*, [*a*+k] and [*y*-k] type fragment ions is important because this confirms the presence of fragment ions produced from a radical-based dissociation mechanism[78–80] at the 2–3 mbar pressure regime we are operating under. We point out that we were unable to identify an abundant ion at *m/z* 381, which warrants further investigations under considerations of sequence-scrambling pathways. Taken together, the data confirm our prior observation[36] that UVPD at 2–3 mbar is feasible and produces fragment ions generally consistent with UVPD carried out under significantly lower pressures.

Next, we characterized the structures of the UVPD-generated fragment ions by their collision cross sections. Most noteworthy is the observation that the [a_6+2] ion is approximately 3% larger in cross section than the a_6 ion, despite only having two additional hydrogen atoms (Figure 1C). Specifically, the a_6 ion appears as two co-existing isomers, as indicated by a broad envelope composed of a main peak (268 Å^2) and a shoulder (260 Å^2). By contrast, the [a_6+2] ion shows a single, main feature at approximately 260 Å^2 (we disregard here the presence of the shoulder for [a_6+2] at ~268 Å^2 because this shoulder is most likely due to the second ^{13}C peak of the a_6 ion; see Figure S4, Supporting Information, for details). Please note that absolute cross section measured in TIMS agree with drift tube values generally to better than 1% and that differences in cross sections of ions within the same spectrum are precise to approximately 0.1 %.[55,66] Hence, this difference in the cross-section is noteworthy because it points to structural differences between the a_6 and [a_6+2] ions that cannot be trivially rationalized by a decrease in mass or by the presence of a chemical moiety that might induce a rearrangement reaction. Furthermore, the ion mobility spectrum of the a_6 ion produced by UVPD differs from that produced by CID (see Figure S4, Supporting Information). Multiple conformations were reported previously for fragment ions generated by MS/MS,[37,41,42] but to our knowledge this is the first observation showing that distinct activation methods could induce different conformations of the same fragment ion. It will be interesting to apply computational techniques to investigate the structural differences between these ions and to reveal their mechanistic origins in upcoming studies. Additionally, we observed two separate isomers for the c_5 ion whereas one main feature predominates for the a_5 and b_5 ions (Figure 1D). The c_5 ion is ~ 3% larger in cross section than the main feature of the a_5 and b_5 ions, which appears unreasonable to rationalize trivially by mere presence of the $-NH_3$ moiety because loss of the -CO group ($b_6 \rightarrow a_5$) does not result in different cross sections. Overall, the recorded ion mobility spectra indicate a rich structural chemistry of the UVPD-generated fragment ions, which will be interesting to investigate in subsequent studies by computational methods as was

previously accomplished for fragment ions related to bottom-up proteomics.[76,81–83] Our results further point to the possibility that cross sections of fragment ions could aid in identification of UVPD-generated fragment ions in line with similar efforts for CID.[38]

Challenges associated with top-down protein analysis at mass tolerances > 1 ppm

Our above discussion confirms prior reports that irradiation of peptides and proteins with UV photons at 2–3 mbar produces sequence-informative fragment ions for polypeptides. Hence, we now discuss application of our instrumental setup for top-down analysis of proteins. In principle, assignment of fragment ions to the detected peaks generated from top-down analysis of proteins in the experiment appears as straight-forward as discussed in Figure 1 for angiotensin I: theoretical fragment ions can be predicted for a polypeptide sequence according to the established cleavage patterns and then assigned to the experimental masses within the instrumental mass accuracy. If the search space of possible fragment ions is limited and the precursor ion is known as in the example above, then this approach can be readily applied to interpret the MS/MS spectra. By contrast, fragment ion assignment can occur by chance if the search space of possible fragment ions is vast and mass accuracy is limited, thereby potentially assigning experimental contaminant or noise peaks as fragment ions.

Table 1 underscores that the fragment ion search space can quickly become significant for top-down analysis even when a single (known) precursor protein is investigated. The table compares the random match probability p at a mass tolerance of 15 ppm for two data sets of fragment ions produced by *in-silico* fragmentation of the respective polypeptide sequence. Here, p denotes the probability that any experimental peak (including noise or contaminants) matches the expected mass of a fragment ion from the polypeptide and is calculated as

$$p = n/h \quad \text{Eq. (1)}$$

where h is the number of bins for the mass range from 100 Da to the neutral polypeptide mass at a given mass tolerance and n is the number of bins associated with fragment ions of the polypeptide sequence. The first set of values was generated from applying the established peptide fragmentation pathways for cleavage of peptide bonds to generate N-terminal (*a, b*) and C-terminal (*y*) fragment ions and their common neutral loss satellite ions ($-NH_3$, $-H_2O$). Even for the 30 kDa protein bovine carbonic anhydrase II, the number of fragment ions appears minor and the probability for a random match at 15 ppm mass accuracy is estimated to a modest ~1.2%. This situation applies to standard CID measurements, but not to the experiments proposed here that couple UVPD with CID in effective MS^3 experiments (see Scheme 1). Hence, our analysis must additionally include internal fragment ions and at least the [*a*+1], [*a*+2], [*y*-1], [*y*-2]-type ions for UVPD. Table 1 underlines that more than 10,000 unique fragment ions can be produced for the 76-residue polypeptide ubiquitin (8.6 kDa), leading to a random match probability of approximately 6% at a mass tolerance of 15 ppm. For the 261-residue protein bovine carbonic anhydrase (30 kDa), we calculated a total of 134,951 unique fragment ions and an estimated 38 %-probability that a contaminant or noise peak in the experiment is randomly assigned as a

fragment ion at a mass tolerance of 15 ppm. Notice that additional considerations of *x* and *z*-type ions, side-chain losses, or post-translational modifications, would further increase the probability for random fragment ion assignments.

Figure 2 reveals how the probability *p* for a random match scales with the instrumental mass accuracy and the polypeptide sequence length. In Figure 2A, we plot *p* for a situation that requires only terminal *a*, *b*, *y* - type fragment ions and their neutral losses to be considered (i.e. CID experiments without abundant formation of internal ions). The data show that under such conditions, reasonably reliable assignment can be accomplished at mass accuracies compatible with IM/MS instruments (i.e. up to ~15–20 ppm). Figure 2B plots the random match probability for a setup coupling CID with UVPD and when internal fragment ions must be considered (excluding *x* and *z*-type ions or side-chains losses). These calculations show that reliable assignment of fragment ions requires mass accuracies of < 100 ppb. Such mass accuracy can be achieved with FT-ICR instruments[84,85] but not on currently available IM/MS instruments that utilize TOF mass analyzers.

To exemplify the challenges of performing reliable top-down protein analysis at mass accuracies compatible with TOF mass analyzers, we plot the random match probability as a function of the peptide sequence length for a mass accuracy of 15 ppm in Figure 2C). The figure shows that fragment ion assignments appear reasonable if CID-type ions (without internal cleavages) are exclusively formed in the experiment. By contrast, if internal ions are considered in conjunction with CID and UVPD-type fragment ions, then the random match probability increases quadratically with sequence length and unambiguous ion assignment at 15 ppm mass accuracy is limited to polypeptides with less than 100 residues. We emphasize that this situation is exacerbated if post-translationally modified protein systems are investigated or if coupling with additional fragmentation methods such as ETD/ECD is performed, further decreasing the effective peptide sequence length that can be reliably analyzed with current TOF mass analyzers.

Automated data analysis workflow for top-down protein analysis coupling tandem-TIMS/MS with UVPD and PASEF MS/MS analysis.

To overcome these limitations and accomplish reliable fragment ion assignment at mass accuracies compatible with our tandem-TIMS/TOF configuration (i.e. in the 5 to 20 ppm range), we take advantage of three properties of our instrumental setup: (1) the ability to record MS/MS spectra resolves ambiguities in ion assignment; (2) the knowledge of the precursor ion mobility and *m/z* ratio limits the possible number of precursor ions for spectral matches; and (3) MS/MS spectra of top-down fragment ions lend themselves ideally for probability-based scoring methods widely used in mass spectrometry-based proteomics.

We thus implemented a data analysis workflow to enable top-down protein analysis based on coupling of CID and UVPD in tandem-TIMS/MS with automated MS/MS acquisition using the PASEF method. Figure 3 illustrates our data analysis workflow for assignment of fragment ions and backbone cleavage patterns using the pentapeptide RPPGF. Figure 3A shows the nested ion mobility / mass spectrum recorded for RPPGF on our tandem-TIMS/MS instrument with mobility-analysis carried out in TIMS-2. The spectrum was recorded under collisional-activating conditions prior to TIMS-2 and shows (fragment)

ions that are mobility-separated in TIMS-2. After mobility-separating the ions in TIMS-2, the PASEF method[57,67] is then used to perform automated MS/MS fragmentation of mobility-selected and *m/z*-selected fragment ions for their sequencing. In the following, we illustrate our data analysis approach using the MS/MS spectrum for fragmentation of the singly-charged precursor ion at *m/z* 573 (see inset, Figure 3A). For illustration of our data processing workflow, we selected *m/z* 573 of the pentapeptide RPPGF because it is the intact precursor ion and its fragment ion spectrum is thus well-suited for unambiguous interpretation.

Compilation of profile MS/MS spectra for top-down fragmentions.—Figure 3B shows the MS/MS spectrum generated by PASEF for the singly charged precursor ion at *m/z* 573. The spectrum was constructed from aggregating the profile spectra for the precursor ion using the application programming interface provided by Bruker Daltonics (see Methods sections). The MS/MS spectrum of *m/z* 573 reveals multiple abundant fragment ions. These fragment ions are manually assigned as sequence-informative *a*, *b*, *y*-type fragment ions produced from cleavage of the peptide backbone as indicated in Figure 3B. The recorded data file further contains information about the precursor ion that was selected for MS/MS fragmentation. Specifically, the PASEF method stores the *m/z* and K_0 ranges for the precursor ions subjected to MS/MS analysis.

Feature detection.—To identify the precursor ion and the produced fragment ions in an automated manner, we first detect features for the MS/MS spectrum. Our approach here applies a continuous wavelet transform (CWT) to detect features in the profile spectrum following prior literature.[86,87] This method produced a set of 10,009 distinct features for the illustrative spectrum shown in Figure 3B.

Feature reduction.—Most of the detected features represent noise or are of such low abundance that they cannot reliably be used for fragment ions assignment. Hence, the next step is to identify the subset of the detected features that contain useful information and to discard those features that obfuscate data interpretation. To this end, our workflow calculates the dynamic noise level (DNL) for each feature following Xu *et al*.[68] as shown in Figure 3C and discards all features with signal/noise ratios smaller than a user-defined threshold *k* (with *k*=3 here). For the illustrative example depicted in Figure 3, only 569 out of the 10,009 detected features (5.5 %) were thus retained for further analysis. Figure 3D shows the line spectrum constructed from the 569 features retained after feature reduction. The spectral similarity between the raw profile spectrum (Figure 3B) and the feature-reduced spectrum (Figure 3D) indicates a significant degree of similarity despite a roughly 95% percent reduction in features.

Charge state deconvolution and determination of monoisotopic masses.—The next data processing step is to identify the monoisotopic masses from the line spectrum. To this end, we use the approach implemented in MSDeconv,[69] which applies a combinatorial algorithm to deconvolve complex spectra with overlapping isotope envelopes produced from top-down protein analysis. Notice that this algorithm has been extensively used in the MASH Explorer suite of programs.[88] For the illustrative example here, MSDeconv

identified monoisotopic masses for 22 ions by deconvolution of the 569 features retained after DNL filtering. Figure 3E shows the deconvolved mass spectrum with only features for the deconvolved monoisotopic masses.

Precursor ion charge state.—For each MS/MS spectrum, the PASEF method records the precursor m/z, K_0, and charge state z, which enables calculation of the precursor ion mass and cross section. Knowledge of the precursor ion mass and cross section is potentially useful for ion assignment because this can be used to constrain the search space of potential precursor ions. We noticed that the PASEF method often incorrectly assigned charge states for larger and highly charged precursor ions (such as y_{67}^{6+} from bovine carbonic anhydrase II discussed later). This challenge is most likely due to the PASEF method being geared towards analysis of short peptide sequences in bottom-up proteomics experiments, whereas our analysis here is typically concerned with precursor polypeptides with on the order of 50 residues and charges states greater than 3+.

To check (and adjust if necessary) the charge state reported by PASEF, we determined the precursor ion charge state from the nested ion mobility / mass spectra (see Figure 3A). To this end, the workflow first applies a CWT to remove high-frequency noise from the nested spectrum as described.[37] Next, the mass spectrum for the m/z and K_0 window associated with the precursor ion is constructed. Finally, the mass spectrum is used to determine the charge state by means of Fourier analysis of its autocorrelation function as described.[89] Based on our experience,[37] this approach reliably assigns charge states even for noisy regions of nested ion mobility/mass spectra.

Assignment of fragment ions.—As discussed above, reliable assignment of the fragment ions in the MS/MS spectra is hampered by the limited mass accuracy achieved by current TOF mass analyzers. Hence, to improve reliability of our fragment ion assignments, we used the OMSSA scoring function[70] to calculate the E-value for the spectral matches, i.e. the probability that the ion assignment is not caused by a random process. We chose to score spectral matches with the OMSSA function here because of its straight-forward software implementation but the Mascot/MascotTD[90] or Sequest[91] scoring methods should be equally applicable. Note that the OMSSA scoring function is based on a Poisson process and mathematically related to the scoring function implemented in the ProSight algorithm,[92] which has been applied with great success for top-down protein analysis. For each MS/MS spectrum, we then scored all putative precursor ions consistent with the precursor ion mass and rank-ordered them by their calculated E-values. Assignments resulting in E-values below a user-defined significance level are discarded from further analysis (see below for estimating a reasonable threshold value using a decoy-sequence strategy).

For the m/z 573 precursor ion for RPPGF shown for illustrative purposes in Figure 3, we found one putative precursor ion (y_5) compatible with the precursor ion. Our data analysis workflow was able to match 13 out of 22 peaks at a mass tolerance of 10 ppm, which resulted in an E-value calculated to $10^{-37.5}$. As indicated in Figure 3F, these assignments account for ~95% of the total ion count in the spectrum and are consistent with our manual assignments shown in Figure 3B.

Automated interpretation of top-down protein analysis by tandem-TIMS/MS coupled with PASEF MS/MS.

To test our data analysis approach described above on a more realistic sample, we analyzed bovine carbonic anhydrase II by tandem-TIMS-PASEF/MS. To this end, we electrosprayed carbonic anhydrase II from denaturing conditions and collisionally-activated the intact ions by placing 180 V between ion apertures L2 and L3 (see Scheme 1 and Figure S1, Supporting Information). Collisional-activation causes bovine carbonic anhydrase II to dissociate into fragment ions, which are subsequently accumulated and separated in TIMS-2 (Figure 4A). To provide a baseline for ion assignment, we first assigned the fragment ions detected in the nested ion mobility / mass spectrum produced by CID of the intact carbonic anhydrase II using ProSight Lite (see Figure S10 in the Supporting Information).[93] The analysis indicates extensive fragmentation at the amino and carboxy termini as expected for CID at an overall cleavage coverage of 32 %. The top-down fragment ions eluting from TIMS-2 were then subjected to the PASEF method for automated precursor ion selection and MS/MS fragmentation as described under Methods. As shown in Figure 4A, multiple precursor ions are successfully selected and subjected to MS/MS analysis.

To exemplify the quality of the recorded MS/MS spectra, Figure 4B shows the MS/MS spectrum recorded for the precursor ion selected at m/z 1267 and $1/K_0$=1.350 with charge state 6+ (additional MS/MS spectra are shown in Figure S12, Supporting Information). The MS/MS spectrum reveals abundant formation of fragment ions between m/z 200 and m/z ~2500. For the spectrum shown in Figure 4B, the data analysis procedure described above recognized monoisotopic masses for 101 ions, many of which have charge states 3+ and 4+. A total of 74 of these experimental ions could be matched to fragment ions of y_{67}^{6+} at a mass tolerance of 5 ppm, resulting in an E-value for y_{67}^{6+} of 10^{-46}. To check assignment of the automated data analysis workflow, we manually confirmed that the predicted isotope patterns of the assigned ions match the experimental data. Notice that y_{67} results from cleavage of the peptide bond N-terminal to Pro93, which highlights presence of the proline-effect[94] and thus further reinforces the assignment. Figure 4B reveals that the ions assigned to the peaks are a, b, y-type fragment ions and that many of the more abundant ions are produced by the proline-effect (e.g. y_{47}^{3+}, y_{47}^{4+}, b_9, and the internal ions b_9, b_{10}, and b_{11} annotated in Figure 4B). These observations further support the validity of the fragment ion assignments.

For automated interpretation of larger data sets, the significance threshold of the obtained E-values must be statistically determined. To assess which E-values are significant for ion assignment, we thus compared E-values calculated for the known amino acid sequence of bovine carbonic anhydrase II to those calculated for the reverse sequence (Figure 4C). This approach was motivated by the established procedure in bottom-up proteomics to use decoy databases with reversed amino acid sequences to establish the significance level of the calculated scores.[95] Hence, we recorded 9 additional data sets and extracted all PASEF MS/MS spectra. Subsequently, we calculated the E-values for all potential precursor ions compatible with the masses of the respective precursor ions, both for the forward and reverse (decoy) amino acid sequences of bovine carbonic anhydrase II.

Figure 4C compares the frequency distribution of the calculated E-values for carbonic anhydrase II to those calculated for its reverse sequence at three mass tolerances (5, 10, 20 ppm). The histograms show that the $-\log E$ values calculated for the carbonic anhydrase sequence generally increase with decreasing mass tolerance. The plots further reveal that the histograms for the carbonic anhydrase II forward (target) sequence exhibit tails at high $-\log E$ values which are not present in the histograms for the reverse (decoy) sequence. Hence, we consider assignments with $-\log E$ values greater than those calculated for the reverse sequence as significant. To assess the significance of these E-values more quantitatively, we calculated the ratio $r(E_0)$ with

$$r(E_0) = \frac{N(E \leq E_0)_{\text{decoy}}}{N(E \leq E_0)_{\text{target}}} \quad \text{Eq. (2)}$$

where $N(E \leq E_0)_{\text{decoy}}$ and $N(E \leq E_0)_{\text{target}}$ refer to the number of spectral matches with an E-value lower than the threshold E_0 for the decoy and target amino acid sequences, respectively. Here, we followed the strategy of estimating the false discovery rate in bottom-up proteomics.[95,96] Figure 4D plots $r(E_0)$ as a function of E_0 for the different mass tolerances. The plot shows that $-\log E$ values greater than approximately 13 to 15 appear reasonable as threshold for assignment of MS/MS spectra for the data sets studied here.

Figure 4E shows the cleavage coverage map generated for the data set shown in Figure 4A using a threshold value of $-\log E_0$ greater than 15 at a mass tolerance of 5 ppm. This data set contains 31 experimental PASEF MS/MS spectra, for which we scored all potential precursor ions and rejected all assignments with $-\log E < 15$. This resulted in precursor ion assignments for 11 out of 31 experimental MS/MS spectra, for which we accepted the highest scoring precursor ion. Accounting for multiple charge states of the same fragment ion, we obtained MS/MS spectra for 8 distinct fragment ions. We subsequently used the fragment ion matches of these precursor ions to generate the cleavage map shown in Figure 4E. The cleavage map shows that 9 out of 11 accepted precursor ions are associated with C-terminal *y*-type fragment ions and two MS/MS spectra were assigned to N-terminal *b*-type ions (b_{36} and b_{40}). Six of these precursor ions (b_{40}, y_{24}, y_{25}, y_{60}, y_{61}, y_{67}; see Figure 4C) are related to the proline-effect, which lends credibility to the precursor assignments. The cleavage map further shows no spectral match for the central region of the amino acid sequence, which is expected for CID-type fragmentation of larger precursor proteins. Hence, the lack of assignments to precursor and fragment ions associated with the central region of the polypeptide sequence further corroborates the reliability of our data analysis approach. Overall, these fragment ion assignments result in a cleavage coverage of 96 out of 259 amide bonds (37% coverage) from the data set shown in Figure 4A, but it should be noted that this coverage mainly stems from fragmentation of only two ions (namely the largest carboxy and amino terminal ions y_{67} and b_{40}).

Next, we assessed the data acquisition time scale required for reliable ion assignment (Figure S6). To this end, we varied the number of PASEF MS/MS spectra that were aggregated for a specific precursor ion and subjected for data analysis and E-value scoring.

Figure S6A indicates that the quality of the aggregated MS/MS spectra still results in significant $-\log E$ values for the y_{61}, y_{67}, and y_{27} fragment ions when only 500 MS/MS scans are aggregated for a specific precursor ion. The resulting cleavage map for the y_{67} precursor ion is shown in Figure S6B, which still appears sufficient as input for BLAST to identify carbonic anhydrase as the protein ion (BLAST E-score of 10^{-10}). Note that our settings recorded 500 PASEF frames (each with up to 10 precursor ion selections) within approximately 2.5 minutes of measurement time, which means that there are ample opportunities to optimize the PASEF settings to either improve the sequence coverage obtained or to reduce the time scale needed for protein identification.

Protein top-down analysis by tandem-TIMS/MS coupled with UVPD and PASEF MS/MS analysis.

Our above discussion underlined the ability of our tandem-TIMS/MS instrument to perform UVPD at 2–3 mbar without generating UV-specific noise peaks at abundances significant enough to hamper data analysis. Further, we described a data processing algorithm that reliably assigns fragment ion matches to PASEF MS/MS spectra in effective MS^3 measurements from an intact precursor protein. We now evaluate the ability of our instrumental configuration of performing top-down protein analysis by coupling tandem-TIMS/MS analysis of an intact protein with UVPD and PASEF MS/MS analysis of the UV-generated and mobility-separated fragment ions (see Scheme 1).

Figure S7A shows the mass spectrum recorded for bovine ubiquitin electrosprayed from ammonium acetate solution with mobility-separation in TIMS-1. We subsequently mobility-selected charge state 6+ by gating the ions eluting from TIMS-1 between apertures L2 and L3 as described (Figure S7B). Next, we stored the selected ions between 10 ms and 100 ms in the quadrupolar ion trap for irradiation with a UV laser that operates at 1000 Hz with pulse energies set to approximately 10 μJ (Figure S7C to S7F). The data reveal that a storage time of 10 ms does not result in abundant formation of fragment ions (Figure S7C) whereas storage times longer than 10 ms appear sufficient to induce fragmentation at the selected laser pulse energy (Figures S7D to S7F). The major fragment ions formed by UV irradiation in Figure S7 can be assigned to a set of terminal *a, b, y* - type ions of ubiquitin (and their radical-produced [*a*+k] and [*y*-k] congeners with k = 1, 2) such as y_{40}^{4+} (*m/z* 1141), y_{66}^{5+} (*m/z* 1489), y_{58}^{4+} (*m/z* 1632), b_{18}^{2+} (*m/z* 1017) and a_{18}^{2+} (*m/z* 1003). Note that the spectra recorded at 50 ms and 100 ms trapping time also show formation of a singly charged species at *m/z* 779 which we are unable to assign by standard fragmentation pathways.

It is intriguing to take a closer look at the ion mobility spectra of the a_{18}^{2+} and $[a_{18} + 2]^{2+}$ ions for the different UV irradiation times (Figure 5, see Figure S9 in the Supporting Information for more details). We make two important observations in Figure 5A, which compares the spectra for the a_{18}^{2+} ions obtained at trap storage times varying from 0 ms to 100 ms. First, the data reveal two features for a_{18}^{2+}, a compact one centered at ~415 $Å^2$ and an extended feature centered at 512 $Å^2$, respectively. This observation implies that the a_{18}^{2+} fragment ions exist in two distinct conformations that (1) are stable on the ~100 ms time scale of the TIMS-2 separation; and (2) differ in cross section by about 20%. Second, the plot shows that no a_{18}^{2+} fragment can be detected without UV irradiation and

that the abundances of the a_{18}^{2+} fragment ions increase with increasing trap storage/UV exposure time. This means that both features are produced from absorption of UV photons. Further, Figure 5B indicates that the relative abundance of the compact feature centered at ~415 $Å^2$ increases with increasing trap storage/UV exposure time. This observation can be rationalized in two ways. For one, the more extended conformation could more efficiently absorb UV photons and undergo secondary fragmentation, especially at prolonged UV irradiation times. Alternatively, the more compact feature could be preferentially formed upon prolonged exposure to UV photons, potentially through a different dissociation mechanism than the extended feature. The plot also shows that the relative abundance of the compact and extended features appear similar for the a_{18}^{2+} and $[a_{18}+2]^{2+}$ fragment ions. Nevertheless, in overall agreement with our discussion above of the a_6 and $[a_6+2]$ fragment ions produced from UVPD of angiotensin I (Figures 1C and 1D) and our analysis of top-down fragment ions reported previously, the spectra in Figure 5 highlight a rich structural chemistry of the fragment ions which could potentially be exploited for their assignments.

For PASEF MS/MS analysis of the UVPD fragment ions separated in TIMS-2 (see Scheme 1), we thus chose a trap storage time of 20 ms for UV exposure to minimize the overall experimental time-scale of coupling two ion mobility separations with MS/MS analysis in a single measurement workflow. Figure 6 summarizes our tandem-TIMS/MS measurements coupling UVPD with PASEF MS/MS analysis. Here, mobility-separations were carried out in TIMS-1 and TIMS-2 over 100 ms and coupled with mobility-selection of charge state 6+, UVPD/storage for 20 ms, and PASEF MS/MS analysis. Figure 6A depicts the base peak chromatogram highlighting the acquisition of precursor ions and MS/MS spectra in alternating segments of 25 seconds and 50 seconds, respectively. The fragment ions obtained by UVPD of the intact ubiquitin ions are separated in TIMS-2 and precursors are selected for PASEF MS/MS analysis (Figures 6B and 6C). The peptide bond cleavages assigned by analysis of the fragment ions observed in the nested ion mobility/mass spectra produced by UVPD of intact ubiquitin (Figure S11, Supporting Information) indicate significant fragmentation throughout the polypeptide chain. Two of these fragment ions were selected as precursor ions for automated MS/MS fragmentation, which our data analysis workflow assigns as b_{18}^{2+} and a_{18}^{2+} (Figure 6D). The analysis of the MS/MS spectra (Figure 6D) reveals that acquisition of MS/MS spectra for about 50 s is sufficient for reliable assignment ($E < 10^{-30}$) of ions with ~20 residues at significant cleavage coverage. We stress that there are ample opportunities for optimizing the PASEF algorithm for top-down protein analysis, such as optimizing the collision energies for CID, which we will report on elsewhere.

Conclusions

We assessed the ability of conducting top-down protein analysis from native solution conditions using our orthogonal tandem-TIMS/MS instrument coupling UVPD with PASEF MS/MS analysis. We conclude from our analysis that:

1. Our instrumental setup does not produce UV-specific noise peaks at abundances significant enough to hamper data analysis and fragment ion assignments.

2. We demonstrated the ability to generate sequence-informative fragment ions for precursor peptide and protein ions in low charge states by their UV photodissociation at 2–3 mbar.

3. We observed multiple conformations of UVPD-induced [*a*+2]-type ions which differ from the conformations of the corresponding *a*-type ions. This highlights a rich structural chemistry of the UVPD-generated fragment ions and indicates that cross sections of fragment ions could aid in identification of UVPD-generated fragment ions. This structural chemistry and its practical value will be the subject of future research.

4. Experiments coupling UVPD and CID for effective MS^3 top-down protein analysis require consideration of internal fragment ions which renders fragment ion assignments at mass tolerances achievable by TOF mass analyzers unreliable.

5. We described a data analysis strategy for automated interpretation of effective MS^3 experiments coupling UVPD and PASEF MS/MS and demonstrated its reliability.

6. Tandem-TIMS/MS workflows coupling two ion mobility-separations with effective MS^3 analyses stages by CID/UVPD and PASEF MS/MS analysis can be carried out at time-scales on the order of 1–3 minutes.

In summary, our discussion here underlines the potential of effective MS^3 workflows that couple tandem-TIMS/MS with UVPD and PASEF MS/MS analysis for top-down analysis of proteins.

Supplementary Material

Refer to Web version on PubMed Central for supplementary material.

ACKNOWLEDGMENT

The authors thank Dr. Stuart Pengelley for helpful discussions on PASEF. The authors thank Dr. Thais Pedrete for assistance in carrying out some of the measurements. This work was supported by the National Institutes of Health under grant R01GM135682 (C.B.) MER, CAW, AT, EMP, and MAP are employees of Bruker Scientific, LLC which produces timsTOF products.

REFERENCES

(1). Yang X; Coulombe-Huntington J; Kang S; Sheynkman GM; Hao T; Richardson A; Sun S; Yang F; Shen YA; Murray RR; Spirohn K; Begg BE; Duran-Frigola M; MacWilliams A; Pevzner SJ; Zhong Q; Trigg SA; Tam S; Ghamsari L; Sahni N; Yi S; Rodriguez MD; Balcha D; Tan G; Costanzo M; Andrews B; Boone C; Zhou XJ; Salehi-Ashtiani K; Charloteaux B; Chen AA; Calderwood MA; Aloy P; Roth FP; Hill DE; Iakoucheva LM; Xia Y; Vidal M Widespread Expansion of Protein Interaction Capabilities by Alternative Splicing. Cell 2016, 164 (4), 805–817. [PubMed: 26871637]

(2). Li YI; van de Geijn B; Raj A; Knowles DA; Petti AA; Golan D; Gilad Y; Pritchard JK RNA Splicing Is a Primary Link between Genetic Variation and Disease. Science 2016, 352 (6285), 600–604. [PubMed: 27126046]

(3). Harper KL; Sosa MS; Entenberg D; Hosseini H; Cheung JF; Nobre R; Avivar-Valderas A; Nagi C; Girnius N; Davis RJ; Farias EF; Condeelis J; Klein CA; Aguirre-Ghiso JA Mechanism of Early

Dissemination and Metastasis in Her2+ Mammary Cancer. Nature 2016, 540 (7634), 588–592. [PubMed: 27974798]

(4). Bludau I; Aebersold R Proteomic and Interactomic Insights into the Molecular Basis of Cell Functional Diversity. Nat. Rev. Mol. Cell Biol 2020, 21 (6), 327–340. [PubMed: 32235894]

(5). Aebersold R; Agar JN; Amster IJ; Baker MS; Bertozzi CR; Boja ES; Costello CE; Cravatt BF; Fenselau C; Garcia BA; Ge Y; Gunawardena J; Hendrickson RC; Hergenrother PJ; Huber CG; Ivanov AR; Jensen ON; Jewett MC; Kelleher NL; Kiessling LL; Krogan NJ; Larsen MR; Loo JA; Ogorzalek Loo RR; Lundberg E; MacCoss MJ; Mallick P; Mootha VK; Mrksich M; Muir TW; Patrie SM; Pesavento JJ; Pitteri SJ; Rodriguez H; Saghatelian A; Sandoval W; Schlüter H; Sechi S; Slavoff SA; Smith LM; Snyder MP; Thomas PM; Uhlén M; Van Eyk JE; Vidal M; Walt DR; White FM; Williams ER; Wohlschlager T; Wysocki VH; Yates NA; Young NL; Zhang B How Many Human Proteoforms Are There? Nat. Chem. Biol 2018, 14 (3), 206–214. [PubMed: 29443976]

(6). Smith LM; Agar JN; Chamot-Rooke J; Danis PO; Ge Y; Loo JA; Paša-Tolić L; Tsybin YO; Kelleher NL; The Consortium for Top-Down Proteomics. The Human Proteoform Project: Defining the Human Proteome. Sci. Adv 2021, 7 (46), eabk0734. [PubMed: 34767442]

(7). Aebersold R; Mann M Mass-Spectrometric Exploration of Proteome Structure and Function. Nature 2016, 537 (7620), 347–355. [PubMed: 27629641]

(8). Smith LM; Kelleher NL Proteoforms as the next Proteomics Currency. Science 2018, 359 (6380), 1106–1107. [PubMed: 29590032]

(9). Yuan Z-F; Arnaudo AM; Garcia BA Mass Spectrometric Analysis of Histone Proteoforms. Annu. Rev. Anal. Chem 2014, 7 (1), 113–128.

(10). He L; Rockwood AL; Agarwal AM; Anderson LC; Weisbrod CR; Hendrickson CL; Marshall AG Top-down Proteomics—a near-Future Technique for Clinical Diagnosis? Ann. Transl. Med 2020, 8 (4), 136–136. [PubMed: 32175429]

(11). Larson EJ; Roberts DS; Melby JA; Buck KM; Zhu Y; Zhou S; Han L; Zhang Q; Ge Y High-Throughput Multi-Attribute Analysis of Antibody-Drug Conjugates Enabled by Trapped Ion Mobility Spectrometry and Top-Down Mass Spectrometry. Anal. Chem 2021, 93 (29), 10013–10021. [PubMed: 34258999]

(12). Toby TK; Fornelli L; Kelleher NL Progress in Top-Down Proteomics and the Analysis of Proteoforms. Annu. Rev. Anal. Chem 2016, 9 (1), 499–519.

(13). Melby JA; Roberts DS; Larson EJ; Brown KA; Bayne EF; Jin S; Ge Y Novel Strategies to Address the Challenges in Top-Down Proteomics. J. Am. Soc. Mass Spectrom 2021, 32 (6), 1278–1294. [PubMed: 33983025]

(14). Compton PD; Zamdborg L; Thomas PM; Kelleher NL On the Scalability and Requirements of Whole Protein Mass Spectrometry. Anal. Chem 2011, 83 (17), 6868–6874. [PubMed: 21744800]

(15). Wu CC; Yates JR The Application of Mass Spectrometry to Membrane Proteomics. Nat. Biotechnol 2003, 21 (3), 262–267. [PubMed: 12610573]

(16). Wang Y; Olesik SV Enhanced-Fluidity Liquid Chromatography–Mass Spectrometry for Intact Protein Separation and Characterization. Anal. Chem 2019, 91 (1), 935–942. [PubMed: 30523683]

(17). Eschelbach JW; Jorgenson JW Improved Protein Recovery in Reversed-Phase Liquid Chromatography by the Use of Ultrahigh Pressures. Anal. Chem 2006, 78 (5), 1697–1706. [PubMed: 16503625]

(18). Liang Y; Jin Y; Wu Z; Tucholski T; Brown KA; Zhang L; Zhang Y; Ge Y Bridged Hybrid Monolithic Column Coupled to High-Resolution Mass Spectrometry for Top-Down Proteomics. Anal. Chem 2019, 91 (3), 1743–1747. [PubMed: 30668094]

(19). Kafader JO; Durbin KR; Melani RD; Des Soye BJ; Schachner LF; Senko MW; Compton PD; Kelleher NL Individual Ion Mass Spectrometry Enhances the Sensitivity and Sequence Coverage of Top-Down Mass Spectrometry. J. Proteome Res 2020, 19 (3), 1346–1350. [PubMed: 32032494]

(20). Polasky DA; Dixit SM; Keating MF; Gadkari VV; Andrews PC; Ruotolo BT Pervasive Charge Solvation Permeates Native-like Protein Ions and Dramatically Influences Top-down Sequencing Data. J. Am. Chem. Soc 2020, 142 (14), 6750–6760. [PubMed: 32203657]

(21). Shaw JB; Li W; Holden DD; Zhang Y; Griep-Raming J; Fellers RT; Early BP; Thomas PM; Kelleher NL; Brodbelt JS Complete Protein Characterization Using Top-Down Mass Spectrometry and Ultraviolet Photodissociation. J. Am. Chem. Soc 2013, 135 (34), 12646–12651. [PubMed: 23697802]

(22). Becher S; Wang H; Leeming MG; Donald WA; Heiles S Influence of Protein Ion Charge State on 213 Nm Top-down UVPD. The Analyst 2021, 146 (12), 3977–3987. [PubMed: 34009215]

(23). Weisbrod CR; Anderson LC; Hendrickson CL; Schaffer LV; Shortreed MR; Smith LM; Shabanowitz J; Hunt DF Advanced Strategies for Proton-Transfer Reactions Coupled with Parallel Ion Parking on a 21 T FT-ICR MS for Intact Protein Analysis. Anal. Chem 2021, 93 (26), 9119–9128. [PubMed: 34165955]

(24). Zinnel NF; Pai P-J; Russell DH Ion Mobility-Mass Spectrometry (IM-MS) for Top-Down Proteomics: Increased Dynamic Range Affords Increased Sequence Coverage. Anal. Chem 2012, 84 (7), 3390–3397. [PubMed: 22455956]

(25). Avtonomov DM; Polasky DA; Ruotolo BT; Nesvizhskii AI IMTBX and Grppr: Software for Top-Down Proteomics Utilizing Ion Mobility-Mass Spectrometry. Anal. Chem 2018, 90 (3), 2369–2375. [PubMed: 29278491]

(26). Stiving AQ; Harvey SR; Jones BJ; Bellina B; Brown JM; Barran PE; Wysocki VH Coupling 193 Nm Ultraviolet Photodissociation and Ion Mobility for Sequence Characterization of Conformationally-Selected Peptides. J. Am. Soc. Mass Spectrom 2020, 31 (11), 2313–2320. [PubMed: 32959654]

(27). Bellina B; Brown Jeffery. M.; Ujma J; Murray P; Giles K; Morris M; Compagnon I; Barran Perdita. E. UV Photodissociation of Trapped Ions Following Ion Mobility Separation in a Q-ToF Mass Spectrometer. The Analyst 2014, 139 (24), 6348–6351. [PubMed: 25349872]

(28). Revercomb HE; Mason EA Theory of Plasma Chromatography/Gaseous Electrophoresis. Review. Anal. Chem 1975, 47 (7), 970–983.

(29). Mason EA; McDaniel EW Transport Properties of Ions in Gases; Wiley-VCH: Weinheim (Germany), 1988.

(30). Berthias F; Thurman HA; Wijegunawardena G; Wu H; Shvartsburg AA; Jensen ON Top-Down Ion Mobility Separations of Isomeric Proteoforms. Anal. Chem 2022, 95, 784–791. [PubMed: 36562749]

(31). Liu FC; Cropley TC; Ridgeway ME; Park MA; Bleiholder C Structural Analysis of the Glycoprotein Complex Avidin by Tandem-Trapped Ion Mobility Spectrometry–Mass Spectrometry (Tandem-TIMS/MS). Anal. Chem 2020, 92 (6), 4459–4467. [PubMed: 32083467]

(32). Borotto NB; Graham KA Fragmentation and Mobility Separation of Peptide and Protein Ions in a Trapped-Ion Mobility Device. Anal. Chem 2021, acs.analchem.1c01188.

(33). Baker ES; Burnum-Johnson KE; Ibrahim YM; Orton DJ; Monroe ME; Kelly RT; Moore RJ; Zhang X; Théberge R; Costello CE; Smith RD Enhancing Bottom-up and Top-down Proteomic Measurements with Ion Mobility Separations. PROTEOMICS 2015, 15 (16), 2766–2776. [PubMed: 26046661]

(34). Gerbasi VR; Melani RD; Abbatiello SE; Belford MW; Huguet R; McGee JP; Dayhoff D; Thomas PM; Kelleher NL Deeper Protein Identification Using Field Asymmetric Ion Mobility Spectrometry in Top-Down Proteomics. Anal. Chem 2021, 93 (16), 6323–6328. [PubMed: 33844503]

(35). Liu FC; Ridgeway ME; Park MA; Bleiholder C Tandem Trapped Ion Mobility Spectrometry. Analyst 2018, 143 (10), 2249–2258. [PubMed: 29594263]

(36). Liu FC; Ridgeway ME; Winfred JSRV; Polfer NC; Lee J; Theisen A; Wootton CA; Park MA; Bleiholder C Tandem-trapped Ion Mobility Spectrometry/Mass Spectrometry Coupled with Ultraviolet Photodissociation. Rapid Commun. Mass Spectrom 2021, 35 (22).

(37). Liu FC; Kirk SR; Caldwell KA; Pedrete T; Meier F; Bleiholder C Tandem Trapped Ion Mobility Spectrometry/Mass Spectrometry (TTIMS/MS) Reveals Sequence-Specific Determinants of Top-Down Protein Fragment Ion Cross Sections. Anal. Chem 2022, 94 (23), 8146–8155. [PubMed: 35621336]

(38). Meier F; Köhler ND; Brunner A-D; Wanka J-MH; Voytik E; Strauss MT; Theis FJ; Mann M Deep Learning the Collisional Cross Sections of the Peptide Universe from a Million Experimental Values. Nat. Commun 2021, 12 (1), 1185. [PubMed: 33608539]

(39). Prianichnikov N; Koch H; Koch S; Lubeck M; Heilig R; Brehmer S; Fischer R; Cox J MaxQuant Software for Ion Mobility Enhanced Shotgun Proteomics. Mol. Cell. Proteomics 2020, 19 (6), 1058–1069. [PubMed: 32156793]

(40). Liu FC; Ridgeway ME; Park MA; Bleiholder C Tandem Trapped Ion Mobility Spectrometry. The Analyst 2018, 143 (10), 2249–2258. [PubMed: 29594263]

(41). Koeniger SL; Merenbloom SI; Valentine SJ; Jarrold MF; Udseth HR; Smith RD; Clemmer DE An IMS−IMS Analogue of MS−MS. Anal. Chem 2006, 78 (12), 4161–4174. [PubMed: 16771547]

(42). Giles K; Ujma J; Wildgoose J; Pringle S; Richardson K; Langridge D; Green M A Cyclic Ion Mobility-Mass Spectrometry System. Anal. Chem 2019, 91 (13), 8564–8573. [PubMed: 31141659]

(43). Kurulugama RT; Nachtigall FM; Lee S; Valentine SJ; Clemmer DE Overtone Mobility Spectrometry: Part 1. Experimental Observations. J. Am. Soc. Mass Spectrom 2009, 20 (5), 729–737. [PubMed: 19195909]

(44). Tang K; Li F; Shvartsburg AA; Strittmatter EF; Smith RD Two-Dimensional Gas-Phase Separations Coupled to Mass Spectrometry for Analysis of Complex Mixtures. Anal. Chem 2005, 77 (19), 6381–6388. [PubMed: 16194103]

(45). Allen SJ; Eaton RM; Bush MF Structural Dynamics of Native-Like Ions in the Gas Phase: Results from Tandem Ion Mobility of Cytochrome c. Anal. Chem 2017, 89 (14), 7527–7534. [PubMed: 28636328]

(46). Eldrid C; Thalassinos K Developments in Tandem Ion Mobility Mass Spectrometry. Biochem. Soc. Trans 2020, 48 (6), 2457–2466. [PubMed: 33336686]

(47). Simon A-L; Chirot F; Choi CM; Clavier C; Barbaire M; Maurelli J; Dagany X; MacAleese L; Dugourd P Tandem Ion Mobility Spectrometry Coupled to Laser Excitation. Rev. Sci. Instrum 2015, 86 (9), 094101. [PubMed: 26429458]

(48). Poyer S; Comby-Zerbino C; Choi CM; MacAleese L; Deo C; Bogliotti N; Xie J; Salpin J-Y; Dugourd P; Chirot F Conformational Dynamics in Ion Mobility Data. Anal. Chem 2017, 89 (7), 4230–4237. [PubMed: 28263061]

(49). Eldrid C; Ben-Younis A; Ujma J; Britt H; Cragnolini T; Kalfas S; Cooper-Shepherd D; Tomczyk N; Giles K; Morris M; Akter R; Raleigh D; Thalassinos K Cyclic Ion Mobility–Collision Activation Experiments Elucidate Protein Behavior in the Gas Phase. J. Am. Soc. Mass Spectrom 2021, 32 (6), 1545–1552. [PubMed: 34006100]

(50). Bleiholder C; Liu FC Structure Relaxation Approximation (SRA) for Elucidation of Protein Structures from Ion Mobility Measurements. J. Phys. Chem. B 2019, 123 (13), 2756–2769. [PubMed: 30866623]

(51). Park MA; Ridgeway M; Bleiholder C; Caroline F Tandem Ion Mobility Spectrometer. US 10,794,861 B2, October 6, 2020.

(52). Liu FC; Ridgeway ME; Park MA; Bleiholder C Tandem-Trapped Ion Mobility Spectrometry/ Mass Spectrometry (t TIMS/MS): A Promising Analytical Method for Investigating Heterogenous Samples. The Analyst 2022, 147 (11), 2317–2337. [PubMed: 35521797]

(53). Kirk SR; Liu FC; Cropley TC; Carlock HR; Bleiholder C On the Preservation of Non-Covalent Peptide Assemblies in a Tandem-Trapped Ion Mobility Spectrometer-Mass Spectrometer (TIMS-TIMS-MS). J. Am. Soc. Mass Spectrom 2019, 30 (7), 1204–1212. [PubMed: 31025294]

(54). Bleiholder C; Liu FC; Chai M Comment on Effective Temperature and Structural Rearrangement in Trapped Ion Mobility Spectrometry. Anal. Chem 2020, 92 (24), 16329–16333. [PubMed: 32578979]

(55). Lee J; Chai M; Bleiholder C Differentiation of Isomeric, Nonseparable Carbohydrates Using Tandem-Trapped Ion Mobility Spectrometry–Mass Spectrometry. Anal. Chem 2022, 95, 747–757. [PubMed: 36547374]

(56). Jeanne Dit Fouque K; Miller SA; Pham K; Bhanu NV; Cintron-Diaz YL; Leyva D; Kaplan D; Voinov VG; Ridgeway ME; Park MA; Garcia BA; Fernandez-Lima F Top-“Double-Down”

Mass Spectrometry of Histone H4 Proteoforms: Tandem Ultraviolet-Photon and Mobility/Mass-Selected Electron Capture Dissociations. Anal. Chem 2022, 94 (44), 15377–15385. [PubMed: 36282112]

(57). Meier F; Beck S; Grassl N; Lubeck M; Park MA; Raether O; Mann M Parallel Accumulation–Serial Fragmentation (PASEF): Multiplying Sequencing Speed and Sensitivity by Synchronized Scans in a Trapped Ion Mobility Device. J. Proteome Res 2015, 14 (12), 5378–5387. [PubMed: 26538118]

(58). Silveira JA; Ridgeway ME; Park MA High Resolution Trapped Ion Mobility Spectrometery of Peptides. Anal. Chem 2014, 86 (12), 5624–5627. [PubMed: 24862843]

(59). Michelmann K; Silveira JA; Ridgeway ME; Park MA Fundamentals of Trapped Ion Mobility Spectrometry. J. Am. Soc. Mass Spectrom 2015, 26 (1), 14–24. [PubMed: 25331153]

(60). Bleiholder C Towards Measuring Ion Mobilities in Non-Stationary Gases and Non-Uniform and Dynamic Electric Fields (I). Transport Equation. Int. J. Mass Spectrom 2016, 399–400, 1–9.

(61). Fernandez-Lima FA; Kaplan DA; Park MA Note: Integration of Trapped Ion Mobility Spectrometry with Mass Spectrometry. Rev. Sci. Instrum 2011, 82 (12), 126106. [PubMed: 22225261]

(62). Silveira JA; Michelmann K; Ridgeway ME; Park MA Fundamentals of Trapped Ion Mobility Spectrometry Part II: Fluid Dynamics. J. Am. Soc. Mass Spectrom 2016, 27 (4), 585–595. [PubMed: 26864793]

(63). Hernandez DR; DeBord JD; Ridgeway ME; Kaplan DA; Park MA; Fernandez-Lima F Ion Dynamics in a Trapped Ion Mobility Spectrometer. Analyst 2014, 139 (8), 1913–1921. [PubMed: 24571000]

(64). Silveira JA; Ridgeway ME; Park MA High Resolution Trapped Ion Mobility Spectrometery of Peptides. Anal. Chem 2014, 86 (12), 5624–5627. [PubMed: 24862843]

(65). Michelmann K; Silveira JA; Ridgeway ME; Park MA Fundamentals of Trapped Ion Mobility Spectrometry. J. Am. Soc. Mass Spectrom 2015, 26 (1), 14–24. [PubMed: 25331153]

(66). Chai M; Young MN; Liu FC; Bleiholder C A Transferable, Sample-Independent Calibration Procedure for Trapped Ion Mobility Spectrometry (TIMS). Anal. Chem 2018, 90 (15), 9040–9047. [PubMed: 29975506]

(67). Meier F; Brunner A-D; Koch S; Koch H; Lubeck M; Krause M; Goedecke N; Decker J; Kosinski T; Park MA; Bache N; Hoerning O; Cox J; Räther O; Mann M Online Parallel Accumulation–Serial Fragmentation (PASEF) with a Novel Trapped Ion Mobility Mass Spectrometer. Mol. Cell. Proteomics 2018, 17 (12), 2534–2545. [PubMed: 30385480]

(68). Xu H; Freitas MA A Dynamic Noise Level Algorithm for Spectral Screening of Peptide MS/MS Spectra. BMC Bioinformatics 2010, 11 (1), 436. [PubMed: 20731867]

(69). Liu X; Inbar Y; Dorrestein PC; Wynne C; Edwards N; Souda P; Whitelegge JP; Bafna V; Pevzner PA Deconvolution and Database Search of Complex Tandem Mass Spectra of Intact Proteins. Mol. Cell. Proteomics 2010, 9 (12), 2772–2782. [PubMed: 20855543]

(70). Geer LY; Markey SP; Kowalak JA; Wagner L; Xu M; Maynard DM; Yang X; Shi W; Bryant SH Open Mass Spectrometry Search Algorithm. J. Proteome Res 2004, 3 (5), 958–964. [PubMed: 15473683]

(71). Brodbelt JS Photodissociation Mass Spectrometry: New Tools for Characterization of Biological Molecules. Chem Soc Rev 2014, 43 (8), 2757–2783. [PubMed: 24481009]

(72). Brodbelt JS Ion Activation Methods for Peptides and Proteins. Anal. Chem 2016, 88 (1), 30–51. [PubMed: 26630359]

(73). Horton AP; Robotham SA; Cannon JR; Holden DD; Marcotte EM; Brodbelt JS Comprehensive *de Novo* Peptide Sequencing from MS/MS Pairs Generated through Complementary Collision Induced Dissociation and 351 Nm Ultraviolet Photodissociation. Anal. Chem 2017, 89 (6), 3747–3753. [PubMed: 28234449]

(74). Greer SM; Brodbelt JS Top-Down Characterization of Heavily Modified Histones Using 193 Nm Ultraviolet Photodissociation Mass Spectrometry. J. Proteome Res 2018, 17 (3), 1138–1145. [PubMed: 29343059]

(75). Zhang L; Reilly JP Extracting Both Peptide Sequence and Glycan Structural Information by 157 Nm Photodissociation of N-Linked Glycopeptides. J. Proteome Res 2009, 8 (2), 734–742. [PubMed: 19113943]

(76). Zabuga AV; Kamrath MZ; Boyarkin OV; Rizzo TR Fragmentation Mechanism of UV-Excited Peptides in the Gas Phase. J. Chem. Phys 2014, 141 (15), 154309. [PubMed: 25338898]

(77). Julian R, The R Mechanism Behind Top-Down UVPD Experiments: Making Sense of Apparent Contradictions. J. Am. Soc. Mass Spectrom 2017, 28 (9), 1823–1826. [PubMed: 28702929]

(78). Morrison LJ; Rosenberg JA; Singleton JP; Brodbelt JS Statistical Examination of the *a* and *a* + 1 Fragment Ions from 193 Nm Ultraviolet Photodissociation Reveals Local Hydrogen Bonding Interactions. J. Am. Soc. Mass Spectrom 2016, 27 (9), 1443–1453. [PubMed: 27206509]

(79). Fornelli L; Srzentić K; Toby TK; Doubleday PF; Huguet R; Mullen C; Melani RD; Dos Santos Seckler H; DeHart CJ; Weisbrod CR; Durbin KR; Greer JB; Early BP; Fellers RT; Zabrouskov V; Thomas PM; Compton PD; Kelleher NL Thorough Performance Evaluation of 213 Nm Ultraviolet Photodissociation for Top-down Proteomics. Mol. Cell. Proteomics 2020, 19 (2), 405–420. [PubMed: 31888965]

(80). Mistarz UH; Bellina B; Jensen PF; Brown JM; Barran PE; Rand KD UV Photodissociation Mass Spectrometry Accurately Localize Sites of Backbone Deuteration in Peptides. Anal. Chem 2018, 90 (2), 1077–1080. [PubMed: 29266933]

(81). Bleiholder C; Osburn S; Williams TD; Suhai S; Van Stipdonk M; Harrison AG; Paizs B Sequence-Scrambling Fragmentation Pathways of Protonated Peptides. J. Am. Chem. Soc 2008, 130 (52), 17774–17789. [PubMed: 19055406]

(82). Harrison AG; Young AB; Bleiholder C; Suhai S; Paizs B Scrambling of Sequence Information in Collision-Induced Dissociation of Peptides. J. Am. Chem. Soc 2006, 128 (32), 10364–10365. [PubMed: 16895391]

(83). Syrstad EA; Turecček F Toward a General Mechanism of Electron Capture Dissociation. J. Am. Soc. Mass Spectrom 2005, 16 (2), 208–224. [PubMed: 15694771]

(84). Lam YPY; Wootton CA; Hands-Portman I; Wei J; Chiu CKC; Romero-Canelon I; Lermyte F; Barrow MP; O'Connor PB Determination of the Aggregate Binding Site of Amyloid Protofibrils Using Electron Capture Dissociation Tandem Mass Spectrometry. J. Am. Soc. Mass Spectrom 2020, 31 (2), 267–276. [PubMed: 31922736]

(85). Palacio Lozano DC; Thomas MJ; Jones HE; Barrow MP Petroleomics: Tools, Challenges, and Developments. Annu. Rev. Anal. Chem 2020, 13 (1), 405–430.

(86). Sturm M; Bertsch A; Gröpl C; Hildebrandt A; Hussong R; Lange E; Pfeifer N; Schulz-Trieglaff O; Zerck A; Reinert K; Kohlbacher O OpenMS – An Open-Source Software Framework for Mass Spectrometry. BMC Bioinformatics 2008, 9 (1), 163. [PubMed: 18366760]

(87). Kohlbacher O; Reinert K; Gröpl C; Lange E; Pfeifer N; Schulz-Trieglaff O; Sturm M TOPP—the OpenMS Proteomics Pipeline. Bioinformatics 2007, 23 (2), e191–e197. [PubMed: 17237091]

(88). Wu Z; Roberts DS; Melby JA; Wenger K; Wetzel M; Gu Y; Ramanathan SG; Bayne EF; Liu X; Sun R; Ong IM; McIlwain SJ; Ge Y MASH Explorer: A Universal Software Environment for Top-Down Proteomics. J. Proteome Res 2020, 19 (9), 3867–3876. [PubMed: 32786689]

(89). Senko MW; Beu SC; McLafferty FW Automated Assignment of Charge States from Resolved Isotopic Peaks for Multiply Charged Ions. J. Am. Soc. Mass Spectrom 1995, 6 (1), 52–56. [PubMed: 24222060]

(90). Karabacak NM; Li L; Tiwari A; Hayward LJ; Hong P; Easterling ML; Agar JN Sensitive and Specific Identification of Wild Type and Variant Proteins from 8 to 669 KDa Using Top-down Mass Spectrometry. Mol. Cell. Proteomics 2009, 8 (4), 846–856. [PubMed: 19074999]

(91). Eng JK; McCormack AL; Yates JR An Approach to Correlate Tandem Mass Spectral Data of Peptides with Amino Acid Sequences in a Protein Database. J. Am. Soc. Mass Spectrom 1994, 5 (11), 976–989. [PubMed: 24226387]

(92). Meng F; Cargile BJ; Miller LM; Forbes AJ; Johnson JR; Kelleher NL Informatics and Multiplexing of Intact Protein Identification in Bacteria and the Archaea. Nat. Biotechnol 2001, 19 (10), 952–957. [PubMed: 11581661]

(93). Fellers Ryan T.; Greer Joseph B.; Early Bryan P.; Yu Xiang; LeDuc Richard D.; Kelleher Neil L.; Thomas. Paul M. ProSight Lite: Graphical Software to Analyze Top-down Mass Spectrometry Data. Proteomics 2014, 15, 1235–1238.

(94). Bleiholder C; Suhai S; Harrison AG; Paizs B Towards Understanding the Tandem Mass Spectra of Protonated Oligopeptides. 2: The Proline Effect in Collision-Induced Dissociation of Protonated Ala-Ala-Xxx-Pro-Ala (Xxx = Ala, Ser, Leu, Val, Phe, and Trp). J. Am. Soc. Mass Spectrom 2011, 22 (6), 1032–1039. [PubMed: 21953044]

(95). Elias JE; Gygi SP Target-Decoy Search Strategy for Increased Confidence in Large-Scale Protein Identifications by Mass Spectrometry. Nat. Methods 2007, 4 (3), 207–214. [PubMed: 17327847]

(96). Lee S; Park H; Kim H Comparison of False-Discovery Rates of Various Decoy Databases. Proteome Sci. 2021, 19 (1), 11. [PubMed: 34537052]

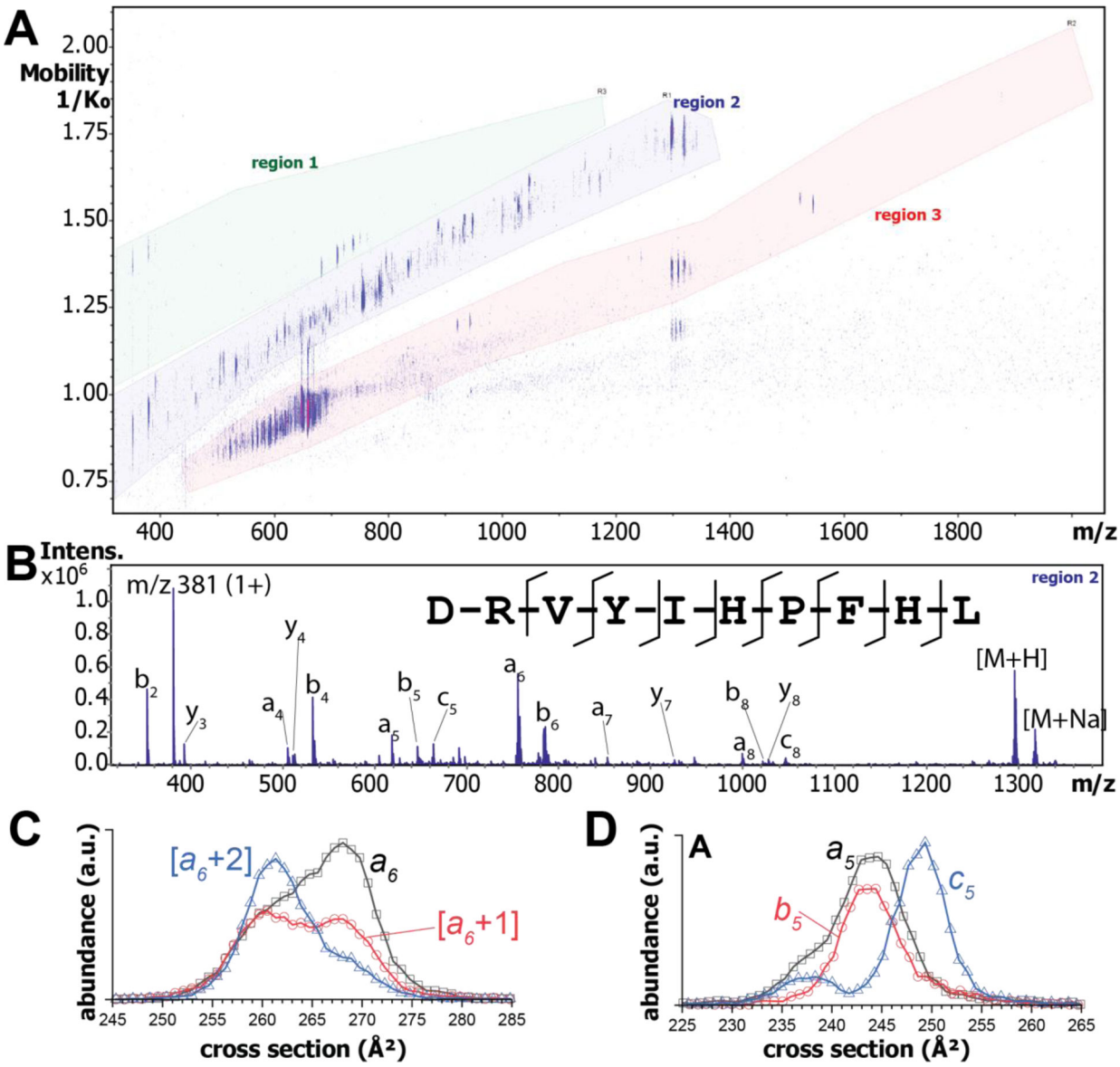

Figure 1.

(A) Nested ion mobility / mass spectrum produced by UVPD for angiotensin I. The spectrum exhibits three bands of ions of which the center band (region 2) is sufficient to obtain the peptide sequence. (B) Extracted mass spectrum for region 2 shown in (A) with fragment ions assigned. (C), (D) Ion mobility spectra for the a_6 fragment ion and its [a+1] and [a+2] congeners and spectra for the a_5, b_5, c_5 ions.

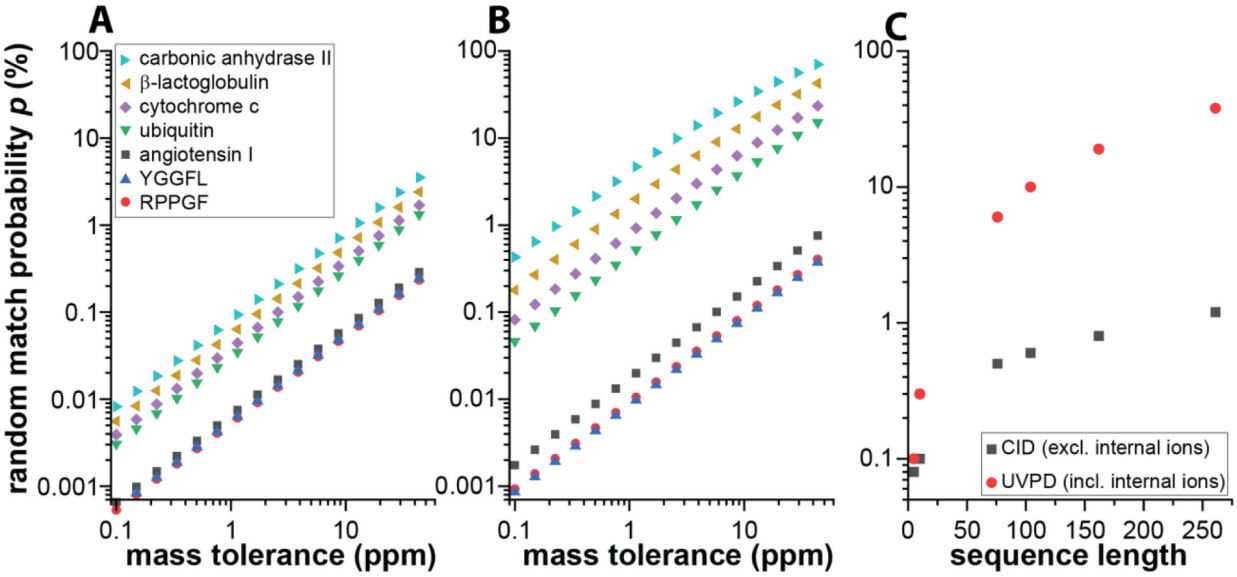

Figure 2.

Random match probability *p* calculated for different polypeptide sequences, mass tolerances, and ion activation methods. The value of *p* denotes the probability that any experimental peak (including noise) would be assigned to a fragment ion at a given mass tolerance. (A) Probabilities considering only terminal *a*, *b*, *y*-type ions and their NH_3, H_2O neutral losses. (B) Random match probabilities considering both internal and terminal *a*, *b*, *y*-type ions and their NH_3, H_2O neutral losses as well as their UVPD-derived [*a*+k] and [*y*-k] congeners (k=1, 2). (C) Random match probabilities as a function of the sequence length at a mass tolerance of 15 ppm compatible with typical TOF mass analyzers. Note the logarithmic scales.

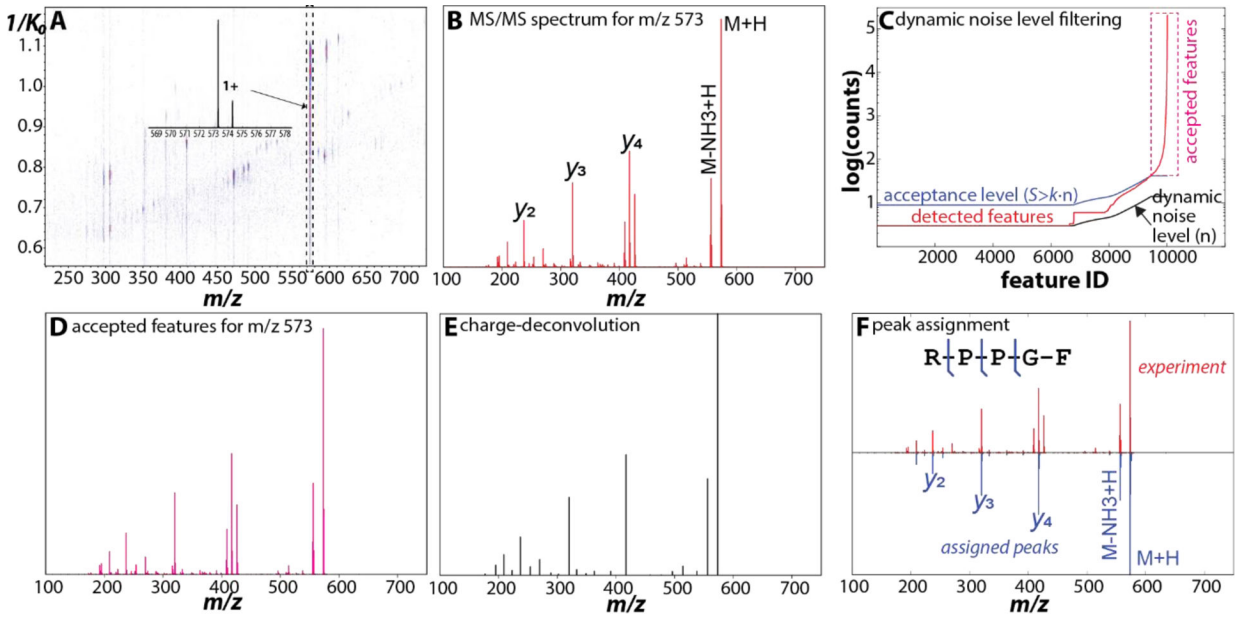

Figure 3.

Illustration of the data analysis algorithm implemented for top-down protein analysis using effective MS3 experiments conducted with tandem-TIMS/MS. (A) Nested ion mobility/mass spectrum showing precursor ion TIMS-MS scans used by the PASEF algorithm to select and schedule ions for MS/MS analysis. (B) PASEF-MS/MS spectrum compiled from a total of 587 individual MS/MS TOF scans for the precursor ion selected at *m/z* 573 and K_0 = 0.978 cm^2/Vs. (C), (D) Features in the experimental MS/MS spectrum are detected by a CWT and subsequently filtered according to their dynamic noise level. (E) Deconvolution and detection of monoisotopic masses is accomplished by MsDeconv. (F) Comparison of the experimental (raw) spectrum and the matched fragment ions. Fragment ions are generated for the input sequence and matched to the experimental monoisotopic masses shown in (E). The OMSSA algorithm is used to score spectral matches.

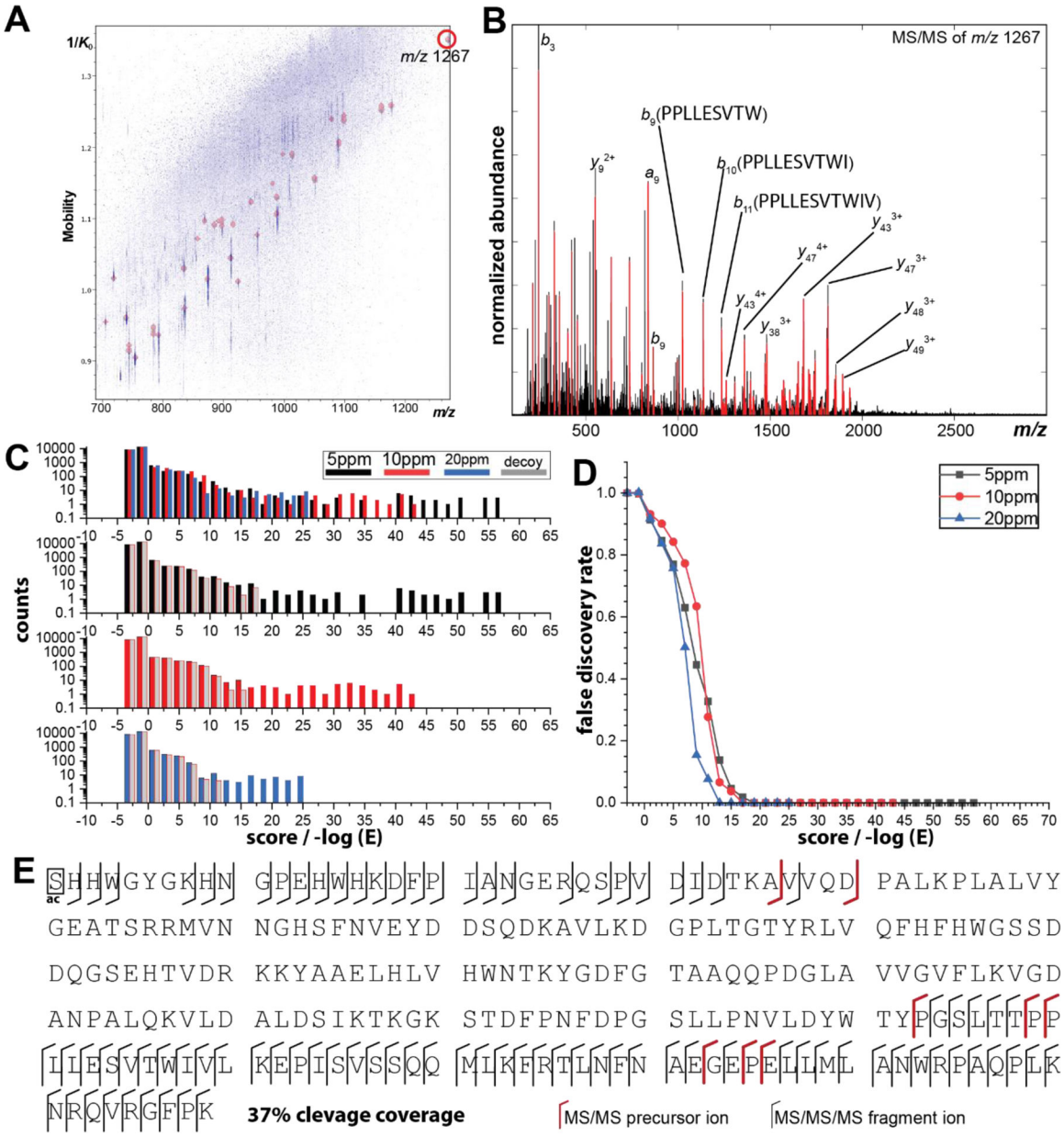

Figure 4.

(A) Fragment ions produced from collisionally-dissociating bovine carbonic anhydrase II are separated in TIMS-2. The markers indicate the *m/z* and K_0 values that were selected for precursor ion selection and automated MS/MS analysis by the PASEF method implemented in the timsTOF Pro. The circle marks the precursor ion corresponding to the PASEF MS/MS spectrum shown in (B). (B). PASEF MS/MS spectrum recorded for precursor ion *m/z* 1267 and $1/K_0$=1.350 cm^2/Vs. The PASEF-recorded charge state of 3+ was corrected to 6+ and the spectrum was assigned to y_{67}^{6+} with a mass of 7598 Da at an E-value of 10^{-46}. Several fragment ion assignments are annotated for illustrative purposes. (C) Distribution of scores calculated for bovine carbonic anhydrase II for the data set shown in Figure 2 at mass tolerances of 5, 10, and 20 ppm. We used the reverse amino acid sequence as decoy. Note

the logarithmic scale of the y-axis. (D) Ratio $r(E_0)$ estimated for the assignments shown in (C) as a function of the threshold score E_0, calculated as the ratio of the respective spectral matches with scores less than E_0 for the decoy and target sequence of carbonic anhydrase II. The plot suggests that precursor ion assignments with scores $-\log E_0$ greater than ~15 are significant at a mass tolerance of 5 ppm. (E) Cleavage map constructed from the data set shown in (A) indicating the accepted PASEF-scheduled precursor ions and their fragment ions. Out of 31 precursor ions selected by PASEF, 11 precursor ions were accepted at a score $-\log E>15$ and assigned to 8 distinct ions, six of which are related to the proline-effect. Notice that the annotated ions do not represent the entire depth of the dataset shown in (A) as only a small subset of the available precursor ions were selected by PASEF.

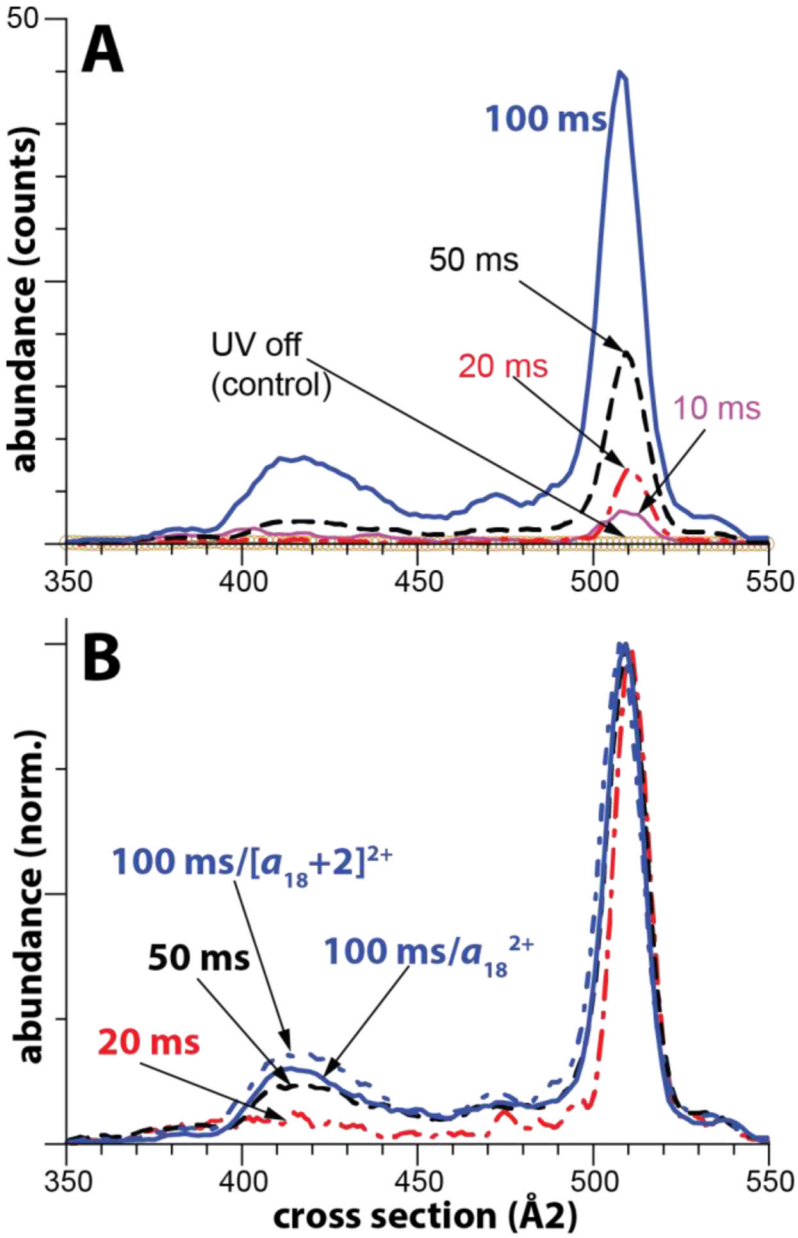

Figure 5.

Ion mobility spectra for a_{18}^{2+} and $[a_{18}+2]^{2+}$ fragment ions obtained by irradiation of bovine ubiquitin 6+ with UV laser pulses at 213 nm at a pulse frequency of 1000 Hz. (A) Spectra for a_{18}^{2+} recorded at different trap storage and UV exposure times reveals presence of two features centered at ~415 $Å^2$ and 512 $Å^2$, respectively. The abundance of a_{18}^{2+} increases with increasing trap storage/UV exposure time. (B) The relative abundance of the compact feature centered at ~415 $Å^2$ increases with increasing trap storage/UV exposure time but does not significantly depend on the apparent formation mechanism (a_{18}^{2+}: blue solid trace; $[a_{18}+2]^{2+}$: red dashed trace).

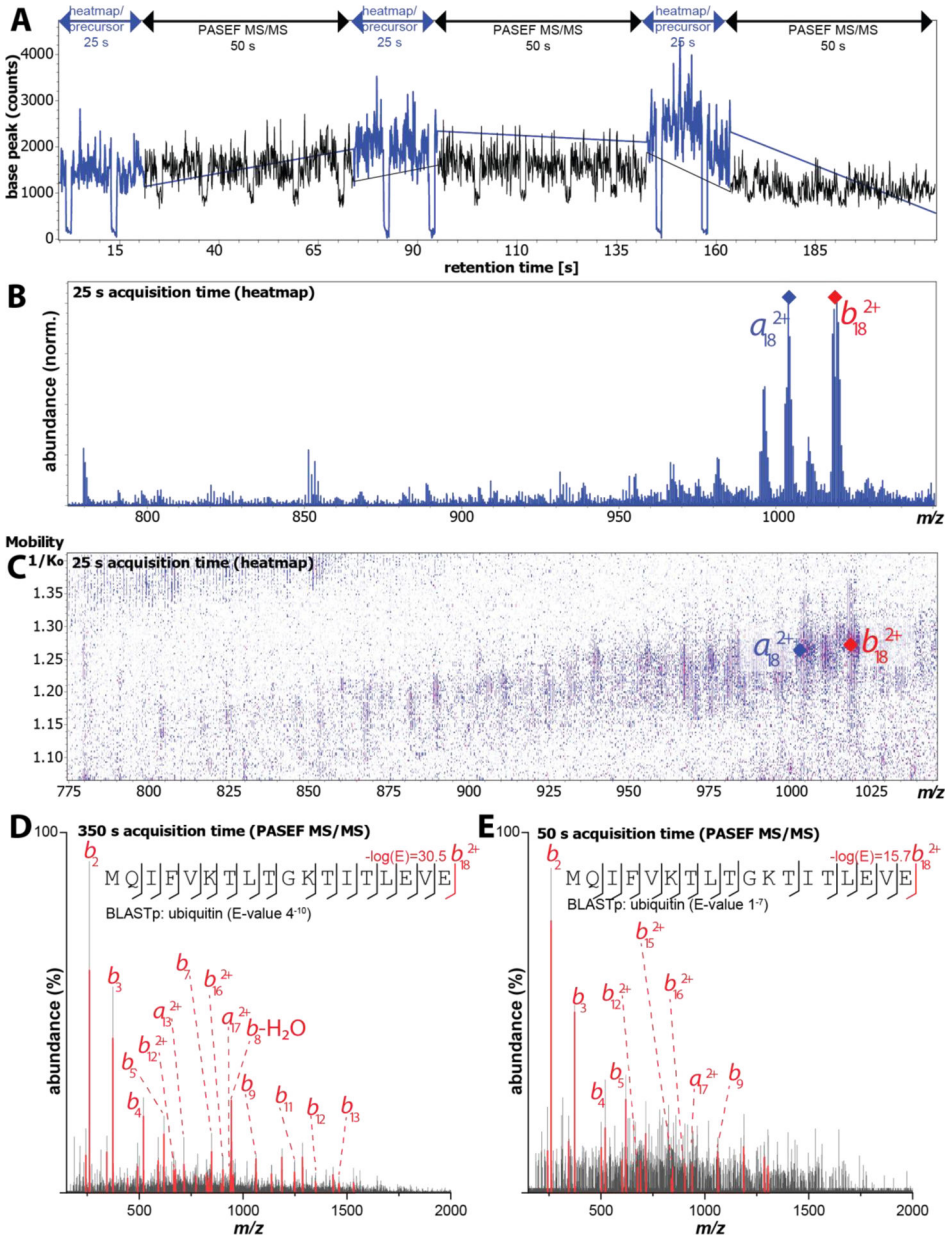

Figure 6.

Tandem-TIMS-UVPD-PASEF/MS analysis of intact ubiquitin charge state 6+ electrosprayed from native solution conditions. (A) Base peak chromatogram highlighting the acquisition of TOF precursor scans (blue trace) used for precursor ion selection and the MS/MS scans (black trace) for the scheduled precursor ions. (B), (C) Mass spectrum and corresponding nested ion mobility/mass spectrum compiled from the TOF precursor scans (blue trace) in (A). The PASEF algorithm scheduled two top-down fragment ions for additional MS/MS analysis, which were subsequently identified by our data analysis strategy as the a_{18}^{2+} (blue diamond) and b_{18}^{2+} (red diamond) fragment ions. (D), (E) PASEF MS/MS spectra for the b_{18}^{2+} fragment ion compiled from aggregating MS/MS scans over a spectra acquisition time window of 350 seconds (D) and 50 seconds (E). Fragment ions were matched (red trace) to

the experimental spectra (black trace) and scored by our data analysis strategy. Both spectra result in reasonable scores and enable BLAST to correctly identify ubiquitin as the precursor protein.

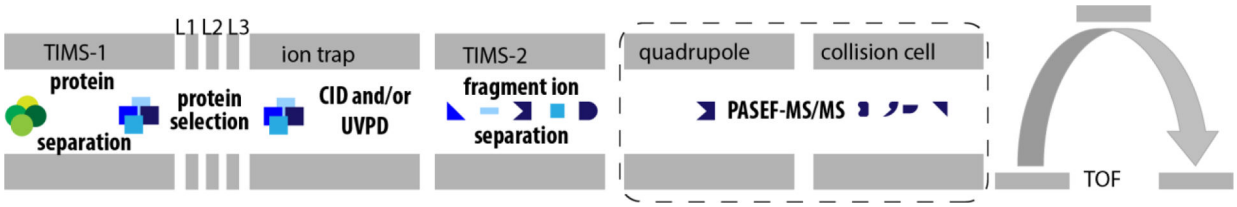

Scheme 1.

Diagram illustrating the sequence of events coupling tandem-TIMS/MS workflows with CID/UVPD and PASEF-MS/MS for top-down protein analysis in effective MS^3 experiments. Proteins are separated in TIMS-1 and mobility-selected for CID or for UVPD in the ion trap. The fragment ions produced are separated in TIMS-2 and subjected to MS/MS analysis by the PASEF method.

Table 1.

Probability for random matches to fragment ions at 15 ppm mass tolerance

Peptide sequence	Sequence length	CID[a]		CID + UVPD[b]	
		Number of primary fragment ions	Random match probability *p* at 15 ppm (%)	Number of primary fragment ions	Random match probability *p* at 15 ppm (%)
RPPGF	5	45	<0.1	77	0.1
angiotensin 1	10	90	0.1	242	0.3
ubiquitin	76	684	0.5	11,792	6.1
cytochrome c	104	936	0.6	21,956	10
β-lactoglobulin	162	1458	0.8	52,986	19
carbonic anhydrase II	261	2331	1.2	134,951	38

[a] considering only terminal *a*, *b*, *y*-type ions including their $-NH_3$ and $-H_2O$ neutral losses

[b] considering terminal *a*, *b*, *y*-type ions and internal *a*, *b*-type ions including their $-NH_3$ and $-H_2O$ neutral losses and their UVPD-generated congeners [*a* +k] and [*y* - k] with k = 1, 2. Not including *c*, *x*, *z*-type ions or side-chain losses.